2018 IEEE International Conference on Robotics and Automation (ICRA)
May 21-25, 2018, Brisbane, Australia

A Nonlinear Control Strategy for Extensible Continuum Robots

Chase G. Frazelle†, Apoorva D. Kapadia, and Ian. D. Walker

Abstract— **In this paper, we describe a novel nonlinear control strategy for the closed-loop control of extensible continuum robots. Previous attempts at controlling continuum robots have proved difficult due to the complexity of their system dynamics. Taking advantage of a previously developed dynamic model for a three-section, planar, continuum manipulator, we develop an adaptation-based control law. We present simulation results of a set-point tracking between a rigid-link control device and an extensible continuum manipulator. Experimental results of the controller implemented on a six degree-of-freedom continuum robot are also presented.**

I. Introduction

Continuum robots [1] have the unique ability to bend at any point along their structure, creating a novel control problem, especially when applying traditional control techniques. This bending ability, derived from the Animal Kingdom (tongues, trunks and tentacles), allows for a range of motions unique to continuum robots that rigid-link manipulators are incapable of performing [2], [3]. There have been numerous designs of continuum systems developed over the years with a corresponding range of potential applications [4], [5], [6], [7], [8], [9], [10], [11], [12].

Continuum robotics is an emerging area of robotics where areas of study common to robotic systems have room to grow and be expanded. Given their ability to navigate unstructured environments [13], wrap around objects of arbitrary shapes [14], and use their entire structure to manipulate an object [15], continuum robots allow for numerous novel applications of robot control theory. One subject that seems to have been largely neglected in continuum robotics literature is the use of nonlinear control techniques.

Kinematic modeling of continuum robots has been the subject of extensive research [16], [17], including the development of Jacobian models, both as approximations [18] and, later, exact models [19], [20], [21]. These models allow for real-time implementation of kinematic control of the often kinematically redundant continuum systems through traditional robot control practices.

Beyond kinematics, dynamic models of continuum systems have been studied and developed [22], [23], [24], [25], [26], [27], [28]. Other works have investigated control applications with dynamic models and model-free control [29], [30], [31], [32], [33], [34], [35]. The development of continuum dynamic models and control using those models currently remain active and open areas of interest and research.

Teleoperative control of continuum robots is another area of investigation in continuum robots that has been investigated [36], [19], [37]. These studies investigated the physical aspect of developing intuitive master systems for the teleoperation of a continuum manipulator. In [38], the work focused on the development of a controller that promoted reduced tracking error between the end-effector positions for kinematically dissimilar master and slave systems through a model-based control law. The investigation of intuitive teleoperation of continuum robots remains an active field of research.

Nonlinear techniques are well established for robotic systems [39], [40], [41]. However, research into the nonlinear control of continuum systems is very limited in the literature. To the authors' knowledge, only one work describes the investigation of nonlinear control methods applied to continuum manipulators [42]. This work was extended and compared to a proportional-derivative controller (PD) in [30]. However, there are still numerous aspects of nonlinear control theory that have yet to be investigated with regard to continuum robotic systems.

In this paper, we introduce a nonlinear control law developed to create asymptotic tracking error convergence between the end-effector of a rigid-link control device and a continuum manipulator in their respective environments. The approach is inspired by adaptive control, but without the need to approximate unmodeled parameters. We report on both simulated and experimental controller performance as measured by the error between a master device and a continuum manipulator.

The paper is organized in the following order: Section II describes the mathematical modeling of the control device and continuum manipulator. Section III describes the development and stability analysis of the implemented control law. Sections IV and V detail simulation and experimental results of the implemented controller. Discussions and conclusions are made in Sections VI and VII, respectively.

II. Mathematical Model

In order to develop the nonlinear control law, we make use of both kinematic and dynamic models of an extensible continuum manipulator limited to a single plane of motion. Specifically, we use the model of a three-section, 9 Degree-of-Freedom (DoF) extensible continuum manipulator referred to as the OctArm [14], seen in Figure 1. The OctArm is a kinematically redundant extensible continuum

† To whom all correspondence should be addressed.
C. G. Frazelle, A. D. Kapadia, and I. D. Walker are with the Dept. of Electrical & Computer Engineering, Clemson University, Clemson, SC-29634-0915 ((cfrazel, akapadi, iwalker)@clemson.edu).
This research was supported by the U.S. NSF under grants IIS-0844954 and IIS-0904116 and by NASA contract NNX12AM01G and by a NASA Space Technology Research Fellowship, contract 80NSSC17K0173.

robot comprised of three serially-connected sections. The sections are designated as the base, middle, and tip, pictured from right to left, respectively, in Figure 1. Each section is capable of three independent motions: change in section length, change in section curvature, and change in orientation in three-dimensional (3D) space.

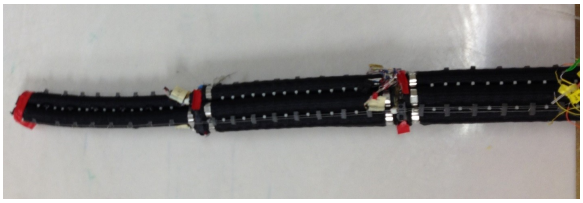

Fig. 1: The 9 Degree-of-Freedom OctArm Manipulator

The 9 DoF available are $q = [s_1\ s_2\ s_3\ \kappa_1\ \kappa_2\ \kappa_3\ \phi_1\ \phi_2\ \phi_3]^{\mathrm{T}}$. As discussed in [17], $s_i(t)$ represents the section length, $\kappa_i(t)$ the section curvature, and $\phi_i(t)$ is the section orientation of the ith section, where i=1, 2, 3. When limited to a single plane, the number of DoF reduces from nine to six, resulting in $q(t) = [s_1\ s_2\ s_3\ \kappa_1\ \kappa_2\ \kappa_3]^{\mathrm{T}}$. Figure 2, from [17], depicts the geometric representation of $s(t)$ and $\kappa(t)$ for a single continuum section.

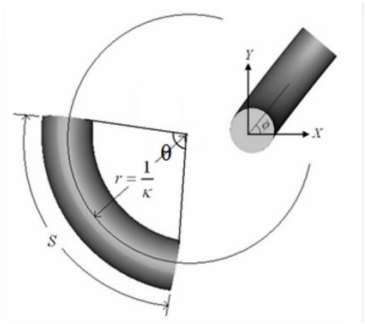

Fig. 2: Geometric Representation of s and κ for Continuum Section

Two master devices were used in this work, one for simulation and one for the physical experiments. The simulation master device is a 2 DoF rigid-link robot composed of two revolute joints. This device can be described by the values $q_m = [\theta_1\ \theta_2]^{\mathrm{T}}$. The physical master device, further described in Section V and [43], is a 9 DoF continuum device kinematically similar to the OctArm.

A. Kinematic Model

The kinematic models of the master device and continuum manipulator are given by:

$$x_i(t) \triangleq f(q_i); i = 1, 2 \tag{1}$$

where $x_i \in \mathbb{R}^{n_i}$ is the position in the task space and $f(q_i) \in \mathbb{R}^{n_i}$ denotes the forward kinematics. The first and second derivatives with respect to time are:

$$\dot{x}_i(t) = J_i \dot{q}_i \tag{2}$$

$$\ddot{x}_i(t) = \dot{J}_i \dot{q}_i + J_i \ddot{q}_i \tag{3}$$

where $J_1 \in \mathbb{R}^{n_1 \times n_1}$ is the Jacobian of the rigid-link master device. The development of the Jacobian for the continuum manipulator can be found in [38].

The homogeneous transformation matrix describing the coordinate frame and orientation transformation to the base plane of a planar, single section continuum [17] robot is given by equation:

$$H = \begin{bmatrix} \cos(s_i\kappa_i) & -\sin(s_i\kappa_i) & 0 & \frac{\cos(s_i\kappa_i)-1}{\kappa_i} \\ \sin(s_i\kappa_i) & \cos(s_i\kappa_i) & 0 & \frac{\sin(s_i\kappa_i)}{\kappa_i} \\ 0 & 0 & 1 & 0 \\ 0 & 0 & 0 & 1 \end{bmatrix} \tag{4}$$

This transformation is used to determine desirable end-effector locations for both the continuum master device and OctArm in simulations by inputting values for $s(t)$ and $\kappa(t)$ and evaluating the Cartesian values obtained from the matrix.

B. Dynamic Model

The dynamic model of the planar continuum manipulator used herein, and detailed in [27], is of the form:

$$M(q)\ddot{q} + C(q, \dot{q})\dot{q} = \tau \tag{5}$$

where $M(q) \in \mathbb{R}^{6\times6}$ is the inertia matrix, $C(q, \dot{q}) \in \mathbb{R}^{6\times6}$ is the Centripetal-Coriolis matrix, and $\tau \in \mathbb{R}^6$ is the control input for the planar continuum manipulator. The variables $\ddot{q}$, $\dot{q}$, and q are the acceleration, velocity, and position of the system. It is assumed that $q(t)$, $\dot{q}(t)$, and $\ddot{q}(t) \in \mathcal{L}_\infty$. The matrix $M(q)$ is symmetric and positive definite and satisfies the following inequalities [44]

$$m_{1i}\|\xi\|^2 \leq \xi^T M_i(\cdot)\xi \leq m_{2i}\|\xi\|^2, \qquad \forall \xi \in \mathbb{R}^6 \tag{6}$$

where m_{1i}, $m_{2i} \in \mathbb{R}$ are positive constants and $\|\cdot\|$ implies the standard Euclidean norm. Further, the matrix $(\dot{M} - 2C)$ is skew-symmetric such that:

$$\xi^T(\dot{M} - 2C)\xi = 0. \qquad \forall \xi \in \mathbb{R}^6 \tag{7}$$

These relationships are exploited when developing the controller.

III. Control Design

The goal of the control design is to cause asymptotic tracking convergence between the end-effector position of the master device and continuum manipulator. Given the simplicity of the two-dimensional (2D) master device, a PD controller is adequate to cause asymptotic convergence to its desired position. For the continuum manipulator, the use of a previously developed Jacobian-based kinematic controller, seen in [17], does eventually allow the end-effector to asymptotically reach the desired position, as illustrated in Figure 5, but does not result in a timely convergence to the solution

required for effective real-time use of the continuum robot. Therefore, it was anticipated that a nonlinear control strategy would be better suited for the control of this inherently nonlinear system.

In order to simplify the modeling, some assumptions were made that further impact the design of the control law. These assumptions are:

1. The continuum manipulator is operating on a plane parallel to the ground, negating the impact of gravity on the dynamic model.

2. The underlying surface on which the continuum manipulator moves is passive and frictionless.

3. The master device is capable of manipulating all the degrees-of-freedom available to the continuum manipulator.

4. The continuum manipulator does not grasp objects, or otherwise contact the environment, to change its mass or dynamic properties.

A. Control Synthesis

In order to create the nonlinear controller, a Lyapunov function was defined for the continuum manipulator system:

$$V(t) \triangleq \frac{1}{2} s^T M s \tag{8}$$

where

$$s(t) = \begin{bmatrix} \dot{\tilde{q}}_1 + \lambda \tilde{q}_1 \\ \dot{\tilde{q}}_2 + \lambda \tilde{q}_2 \\ \dot{\tilde{q}}_3 + \lambda \tilde{q}_3 \\ \dot{\tilde{q}}_4 + \lambda \tilde{q}_4 \\ \dot{\tilde{q}}_5 + \lambda \tilde{q}_5 \\ \dot{\tilde{q}}_6 + \lambda \tilde{q}_6 \end{bmatrix}, \tag{9}$$

where the coefficient λ is a positive, real-valued constant. The values $\dot{\tilde{q}}_i$ and $\tilde{q}_i$ are velocity and position errors between the continuum manipulator and the desired position defined as:

$$\dot{\tilde{q}}_i = \dot{q}_i - \dot{q_{di}}, \tag{10}$$

$$\tilde{q}_i = q_i - q_{di}, \tag{11}$$

where q_{di} and $\dot{q_{di}}$ are the desired position and velocity of the ith control parameter for the continuum manipulator. Further, we find the time derivative of the Lyapunov function as:

$$\dot{V} = \frac{1}{2} s^T M \dot{s} + \frac{1}{2} \dot{s}^T M s + \frac{1}{2} s^T \dot{M} s \tag{12}$$

$$= s^T M \dot{s} + \frac{1}{2} s^T \dot{M} s. \tag{13}$$

Here $\dot{s}(t)$ is

$$\dot{s} = \ddot{q} - \ddot{q_r}, \tag{14}$$

defining the variable $\ddot{q_r} \triangleq \ddot{q_d}$ - $\lambda \dot{\tilde{q}}$. By substituting equation (14) into the derivative of the Lyapunov function in Equation (12), we obtain:

$$\dot{V} = s^T M (\ddot{q} - \ddot{q_r}) + \frac{1}{2} s^T \dot{M} s \tag{15}$$

$$= s^T (\tau - M \ddot{q_r} - C \dot{q}) + \frac{1}{2} s^T \dot{M} s \tag{16}$$

Finally, using the definition $\dot{q} \triangleq s$ + $\dot{q_r}$ and substituting into equation (15), we have the derivative of the Lyapunov function as:

$$\dot{V} = s^T (\tau - M \ddot{q_r} - C(s + \dot{q_r})) + \frac{1}{2} s^T \dot{M} s \tag{17}$$

$$= s^T (\tau - M \ddot{q_r} - C \dot{q_r}) + \frac{1}{2} s^T (\dot{M} - 2C) s \tag{18}$$

$$= s^T (\tau - M \ddot{q_r} - C \dot{q_r}) \tag{19}$$

The term $\frac{1}{2} s^T (\dot{M} - 2C) s$ in equation (18) is zero due to the skew-symmetric property of $(\dot{M} - 2C)$ given in equation (7).

In traditional adaptive control, the results from equation (17) can be used to create an estimate of unknown manipulator variables, such as mass at the end-effector. However, in this research, all parameters are assumed to be known due to the passive environment and Assumption 4. Thus, we simply need to design a control input that can ensure asymptotic tracking convergence and provide stability, the following control law is proposed:

$$\tau = M(\ddot{q_d} - 2\lambda \dot{\tilde{q}} + \lambda^2 \tilde{q}) + C \dot{q_r}, \tag{20}$$

where $\tau \in \mathbb{R}^6$.

B. Stability Result

Before implementing the control law, the stability of the system needs to be determined. First, substituting equation (20) into equation (17) for τ yields:

$$\dot{V} = s^T (M \ddot{q_d} - 2\lambda M \dot{\tilde{q}} + \lambda^2 M \tilde{q} + C \dot{q_r} - M \ddot{q_r} - C \dot{q_r}) \tag{21}$$

$$= s^T (M \ddot{q_d} - 2\lambda M \dot{\tilde{q}} + \lambda^2 M \tilde{q} - M(\ddot{q_d} - \lambda \dot{\tilde{q}})) \tag{22}$$

$$= s^T M (-\lambda \dot{\tilde{q}} - \lambda^2 \tilde{q}) \tag{23}$$

$$= -s^T (\lambda M) s \tag{24}$$

Because M is a positive definite matrix and λ is a positive constant, the term $-s^T(\lambda M)s$ negative-definite. Coupled with the positive-definite nature of the Lyapunov function in equation (8), $\dot{V} \to 0$, thus the solution is determined to be asymptotically stable in the sense of Lyapunov.

IV. Controller Simulation

Simulations were run to test the effectiveness of the control law. A simulated dynamic model of the OctArm with planar motion was first used to test the convergence of the Jacobian-controlled OctArm compared to convergence of the continuum manipulator using the nonlinear control input. In order to ensure an end-effector position achievable by the OctArm, the desired position for simulation was determined by selecting a random OctArm configuration and then using the OctArm forward kinematics to calculate the resulting

end-effector location. For the simulation set reported below, the desired OctArm configuration was set to be:

$$q_d = \begin{bmatrix} s_1 \\ s_2 \\ s_3 \\ \kappa_1 \\ \kappa_2 \\ \kappa_3 \end{bmatrix} = \begin{bmatrix} 0.3233 & m \\ 0.5000 & m \\ 0.4250 & m \\ 0.040 & m^{-1} \\ -0.020 & m^{-1} \\ 0.052 & m^{-1} \end{bmatrix}$$

Using the OctArm forward kinematics for a three-section continuum robot, the desired end-effector location for the OctArm configuration was determined to be:

$$p = \begin{bmatrix} z \\ x \end{bmatrix} = \begin{bmatrix} 1.248 & m \\ -0.012 & m \end{bmatrix}$$

where $z \in \mathbb{R}$ and $x \in \mathbb{R}$ are the coordinates for the base frame, illustrated as z_0 and x_0 in Figure 3.

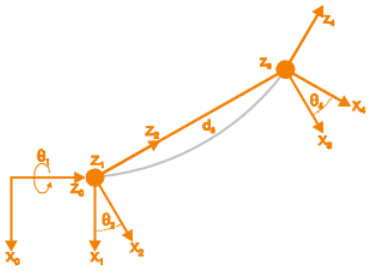

Fig. 3: OctArm Coordinate System

The tracking error of the simulated master device to the desired position can be seen in Figure 4, where asymptotic convergence is achieved through the use of the inverse Jacobian for the 2 DOF rigid-link manipulator. Figure 5 depicts the error tracking between the master device and continuum manipulator when relying on the inverse Jacobian of the OctArm to control its end-effector's location. These errors do eventually converge to the master device's end-effector location with a steady state error of approximately 5 mm, but convergence is not smooth and takes an *a priori* unpredictable amount of time.

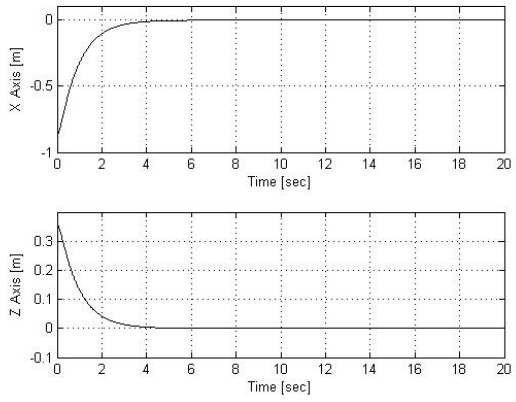

Fig. 4: Rigid-Link Master Device Tracking Error

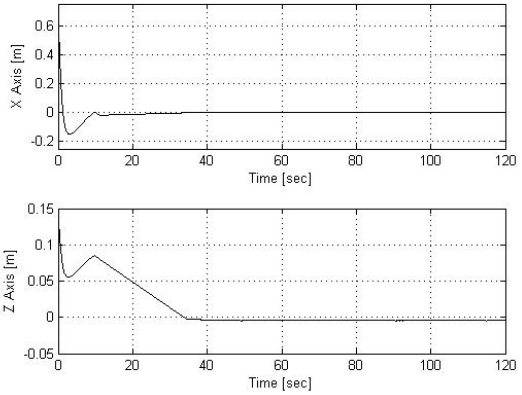

Fig. 5: Jacobian Controlled Simulated OctArm Tracking Error

Figures 6 and 7 depict the corresponding tracking errors between the rigid-link master device and continuum manipulator with the implementation of the nonlinear controller for different values of λ. As can be seen, the time of convergence and the oscillation of the error decreases as the value of λ increases. Setting λ = 1 gives initial convergence to the desired position but results in a steady state error of approximately 18 cm. A value of λ = 25 was found to produce an asymptotically converging tracking error while also eliminating oscillations seen in lower values of λ.

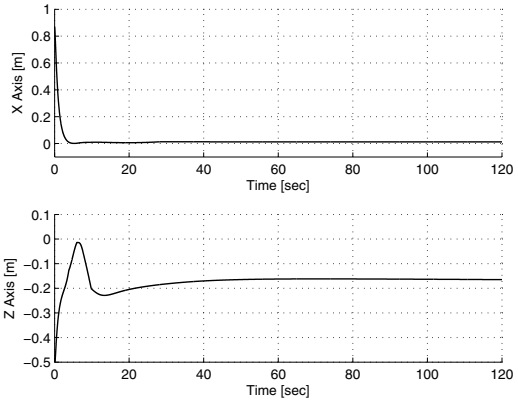

Fig. 6: Simulated OctArm Tracking Error, λ=1

In order to simulate a noisy system feedback in a physical system, an additional simulation was performed with Additive Gaussian white noise introduced into the feedback loop of the system. The Signal to Noise Ratio (SNR) of the Gaussian input was 30 dB, the impact of which can be seen in Figure 8. The end-effector tracking error can still be observed asymptotically converging to zero despite the noise added to the system.

V. Experimental Implementation

In order to validate the controller on a physical continuum manipulator, experiments were conducted using the OctArm. The input device used was a 9 DoF continuum master device, described in [43]. The master device is kinematically similar

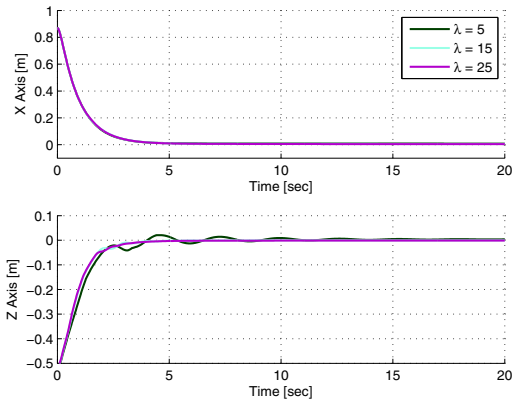

Fig. 7: Simulated OctArm Tracking Error, λ = 5

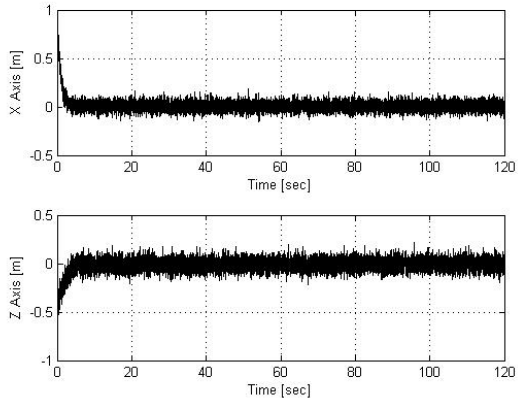

Fig. 8: System Response with added White Gaussian Noise, SNR = 30 dB

to the OctArm, comprised of three sections, each described by $s(t)$, $\kappa(t)$, and $\phi(t)$. In these experiments, only the arc length (s) and curvature (κ) values determined by the master device were used. All three sections of the OctArm were programmed to curve in the same plane.

The nonlinear controller was implemented in Matlab/Simulink [45]. A pair of Quanser Q8 data acquisition boards [46] were used to receive the desired configuration set by the master device and output the values calculated by the nonlinear controller. The kinematic values determined by the master device were used as a desired end-effector set-point location within the Simulink model similar to the set-point used in the simulations in Section IV.

Five configurations were chosen to highlight the effectiveness of the nonlinear controller. These were as follows:

1. No extension or curvature for any section.
2. Base section extended and curved.
3. Middle section extended and curved.
4. Tip section extended and curved.
5. All sections extended and curved.

The specific kinematic values set by the master device for each of the configurations are listed in Table I.

For comparison, the same configurations were used in an open-loop control scheme of the OctArm. Figures 10-14 display both the end-effector error and tracking data for each configuration from both the open-loop and nonlinear closed-loop controller. The tracking plots display the paths traveled by the ends of the base, middle, and tip sections of the OctArm. These paths are colored cyan, green, and red, respectively. Also displayed are the desired set points of the base, middle, and tip section given by the master device. These appear as blue, dark green, and maroon stars. The black triangle marks the beginning of the base section for both the master device and OctArm and a black star designates the final end-effector position for the OctArm.

Parameter	CFG 1	CFG 2	CFG 3	CFG 4	CFG 5
s_{base} [m]	0.3234	0.3600	0.3233	0.3233	0.3437
s_{mid} [m]	0.3140	0.3140	0.3496	0.3140	0.3386
s_{tip} [m]	0.3387	0.3387	0.3387	0.3791	0.3623
κ_{base} [m^{-1}]	0.0012	0.0178	0.0012	0.0012	0.0160
κ_{mid} [m^{-1}]	0.0015	0.0083	0.0392	0.0015	0.0445
κ_{tip} [m^{-1}]	0.0047	0.0047	0.0047	0.0378	0.0296

TABLE I: Kinematic Values for Experimental OctArm Configurations

Additionally, in order to evaluate potential error in system feedback and state estimation, the location of the OctArm end-effector was manually measured using a grid located in the plane-of-motion of the OctArm, as seen in Figure 9. These errors are discussed in Section VI

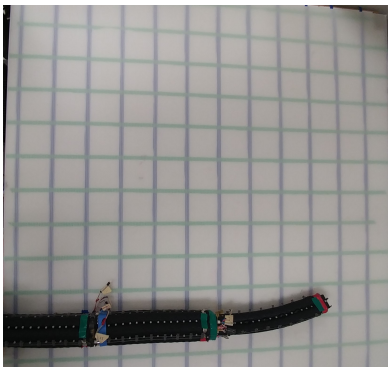

Fig. 9: Experimental Measurement Grid for OctArm

VI. Discussion

A. Simulation Results

The developed control law successfully resulted in asymptotic tracking convergence between the rigid-link master device and continuum manipulator in simulation. As seen in the simulation results, Figures 6 and 7, an increase in the value of λ greatly influenced the accuracy and rate of convergence of the continuum manipulator. Small values of λ ($\lambda \leq 1$) caused the end-effector to over-shoot the desired position and resulted in either oscillating or constant error from the desired position. Larger values of λ ($\lambda > 1$) resulted in ideal asymptotic convergence, though moderate values of λ still produced small amounts of oscillation in the approach to zero-tracking error. Additionally, the continuum manipulator was still able to asymptotically converge to the

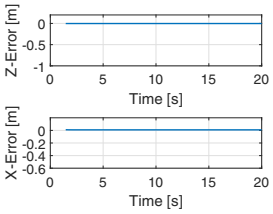

(a) Nonlinear End-Effector Error

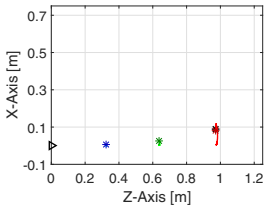

(b) Nonlinear Tracking Data

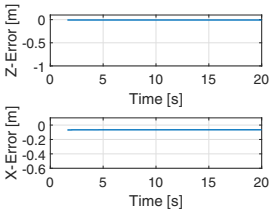

(c) Open Loop End-Effector Error

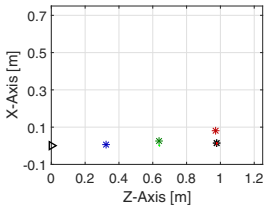

(d) Open Loop Tracking Data

Fig. 10: Straight Configuration Tracking and Error Data

solution despite the presence of Gaussian white noise in the system feedback loop.

B. Experimental Results

During the implementation of the nonlinear controller on the OctArm, multiple considerations were made when obtaining and analyzing the results. Most notable was the need to use a vector of varying λ values for each configuration in order to critically-damp the system response. During simulation, a single λ value for all 6 DoF was adequate for end-effector convergence. In experimentation, a single λ value assigned to the entire OctArm, or even a single section, produced an oscillatory response. Therefore, a vector of 6 λ values, one for each DoF, was implemented. The λ values used to produce the results in Section V varied for each configuration. These values are listed in Table II.

Parameter	CFG 1	CFG 2	CFG 3	CFG 4	CFG 5
s_{base}	85	60	200	600	60
s_{mid}	85	200	380	300	60
s_{tip}	85	200	120	700	60
κ_{base}	85	450	200	1000	550
κ_{mid}	85	200	450	700	600
κ_{tip}	85	200	160	1500	650

TABLE II: λ Values Corresponding to Experimental Configurations

The error and tracking plots in Section V reveal steady-state errors in end-effector location and section end-point locations. These errors can be attributed to a multitude of factors such as imperfections in system feedback, unmodeled friction, physical limitations associated with continuum systems, and model errors.

The error between the manual measurements and state estimate values are seen in Table III. In configuration 4, the curving of the tip section, the error between the manual measurement and the state estimate at the end-effector location

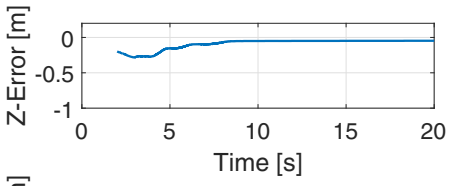

(a) Nonlinear End-Effector Error

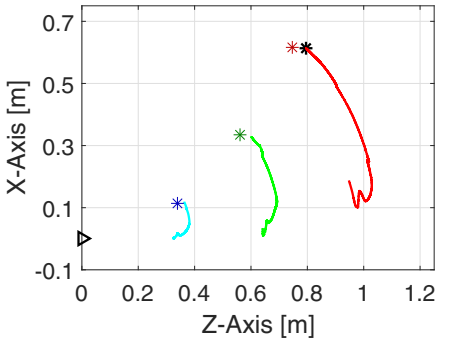

(b) Nonlinear Tracking Data

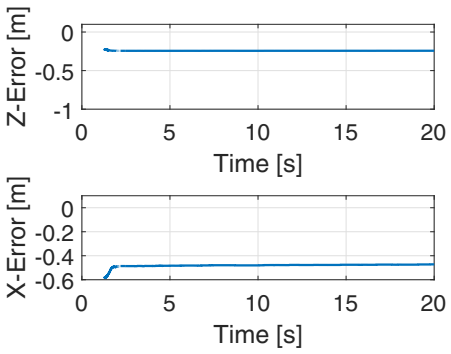

(c) Open Loop End-Effector Error

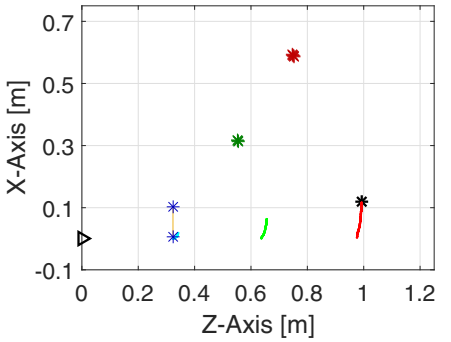

(d) Open Loop Tracking Data

Fig. 11: Curving Base Section Configuration Tracking and Error Data

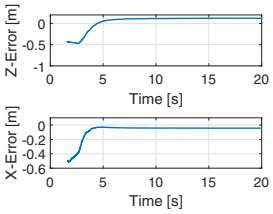

(a) Nonlinear End-Effector Error

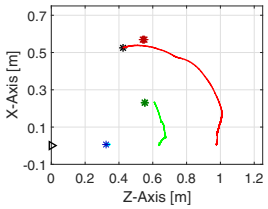

(b) Nonlinear Tracking Data

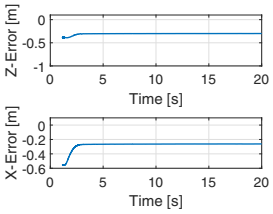

(c) Open Loop End-Effector Error

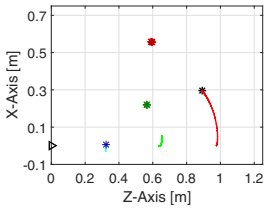

(d) Open Loop Tracking Data

Fig. 12: Curving Middle Section Configuration Tracking and Error Data

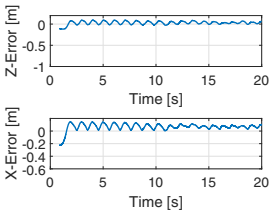

(a) Nonlinear End-Effector Error

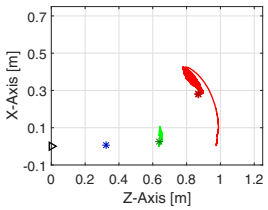

(b) Nonlinear Tracking Data

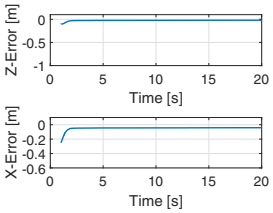

(c) Open Loop End-Effector Error

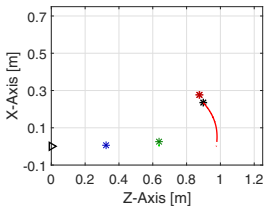

(d) Open Loop Tracking Data

Fig. 13: Curving Tip Section Configuration Tracking and Error Data

could not be captured due to the oscillations seen in Figure 13a.

The limit cycles (oscillations) seen in Figure 13 are likely due to the unmodeled dynamics resulting from our experimental conditions and differences between the physical system and the ideal model used. Corrections made to the model as well as changes to initial conditions could reduce or eliminate these oscillations.

C. Further Research

Further consideration can be given to implementing the developed control law for real-time tracking between a master device and continuum manipulator instead of set point-convergence. This will include the need to dynamically alter λ values during runtime and increase the accuracy of

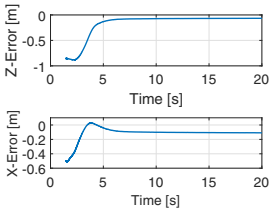

(a) Nonlinear End-Effector Error

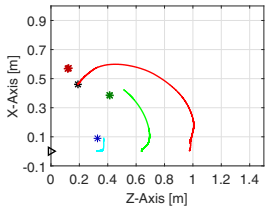

(b) Nonlinear Tracking Data

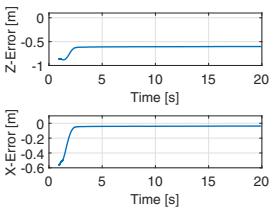

(c) Open Loop End-Effector Error

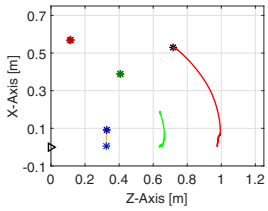

(d) Open Loop Tracking Data

Fig. 14: All Sections Curving Configuration Tracking and Error Data

Parameter	Z-Error [m]	X-Error [m]
CFG 1	0.08	0.07
CFG 2	0.02	0.09
CFG 3	0.03	0.12
CFG 4	-	-
CFG 5	0.01	0.10

TABLE III: State Estimation Error

the dynamic model. One possible solution for this is the implementation of a Kalman filter or similar tool to update λ depending on tracking error.

While the implemented control law performs as desired, there is still the desire to develop a truly adaptive control law for the control of continuum systems. Future work will examine the introduction of uncertainties into the models and environment, such as obstacles and objects to manipulate, as well as friction.

Additionally, there is the need to expand the control of a continuum system to the dimension outside of the plane. This requires the development of a spatial dynamic model capable of modeling all of the degrees-of-freedom available to a three-section continuum robot. Once developed, nonlinear controllers such as the one examined in this paper can be updated to include such a model.

VII. Conclusion

We have introduced a novel nonlinear control law for extensible continuum robots. The control law is inspired by standard adaptive control techniques. However, the control law assumes no uncertainties in the model or the environment. Though the designed control law does not perfectly cancel the continuum manipulator dynamics, the results demonstrate that asymptotic tracking convergence is still achieved at a rate similar to exact cancellation. Results were demonstrated through both the simulation and physical implementation of a three section continuum manipulator. Accompanying this paper is a video showing the tracking

motion of the OctArm in the plane as reported in the experimental results.

REFERENCES

[1] G. Robinson and J. Davies, "Continuum robots - a state of the art," in *Proc. IEEE Int. Conf. Robot. Autom.*, Detroit, MI, 1999, pp. 2849–2854.

[2] R. Webster III and B. A. Jones, "Design and modeling of constant curvature continuum robots," *Int. Jour. Robots. Res.*, vol. 29, no. 13, pp. 1661–1683, Jul. 2010.

[3] D. Trivedi, C. Rahn, W. Kier, and I. Walker, "Soft robotics: Biological inspiration, state of the art, and future research," *Applied Bionics and Biomechanics*, vol. 5, no. 2, pp. 99–117, Jun. 2008.

[4] I. Walker, "Continuous backbone "continuum" robot manipulators: A review," *ISRN Robotics*, vol. 2013, no. 1, pp. 1–19, Jul. 2013.

[5] E. Butler, R. Hammond-Oakley, S. Chawarski, A. Gosline, P. Codd, T. Anor, J. Madsen, P. Dupont, and J. Lock, "Robotic neuro-endoscope with concentric tube augmentation," in *Proc. IEEE/RSJ Int. Conf. Intel. Robot. Syst.*, Vilamoura, Portugal, 2012, pp. 2941–2946.

[6] Y. Chen, J. Liang, and I. Hunter, "Modular continuum robotic endoscope design and path planning," in *Proc. IEEE Int. Conf. Robot. Autom.*, Hong Kong, China, 2014, pp. 5393–5398.

[7] N. Simaan, R. Taylor, and P. Flint, "A dextrous system for laryngeal surgery," in *Proc. IEEE Int. Conf. Robot. Autom.*, New Orleans, LA, 2004, pp. 351–357.

[8] J. Mehling, M. Diftler, M. Chu, and M. Valvo, "A minimally invasive tendril robot for in-space inspection," in *Proc Biorobotics Conference*, Pisa, Italy, 2006, pp. 690–695.

[9] M. Tonapi, I. Godage, A. Vijaykumar, and I. Walker, "Spatial kinematic modeling of a long and thin continuum robotic cable," in *Proc. IEEE Int. Conf. Robot. Autom.*, Seattle, WA, 2015, pp. 3755–3761.

[10] C. Laschi, B. Mazzolai, V. Mattoli, M. Cianchetti, and P. Dario, "Design of a biomimetic robotic octopus arm," *Bioinsp. and Biomim.*, vol. 4, no. 1, pp. 1–8, Jan. 2009.

[11] D. Lane, B. Davies, G. Robinson, D. O'Brien, J. Sneddon, E. Seaton, and A. Elfstrom, "Aspects of the design and development of a subsea dextrous grasping system," *IEEE Jour. Ocean. Eng.*, vol. 24, no. 1, pp. 96–111, Jan. 1999.

[12] R. Buckingham and A. Graham, "Snaking around a nuclear jungle," *Ind. Robot: An Int. Jour.*, vol. 32, no. 2, pp. 120–127, Feb. 2005.

[13] G. Chen, T. Pu, T. Herve, and C. Prelle, "Design and modeling of a micro-robotic manipulator for colonoscopy," in *Proc. SICE Ann. Conf.*, Annecy, France, 2005, pp. 109–114.

[14] M. Grissom, V. Chitrakaran, D. Dienno, M. Csencsits, M. Pritts, B. Jones, W. McMahan, D. Dawson, C. Rahn, and I. Walker, "Design and experimental testing of the octarm soft robot manipulator," in *Proc. SPIE Conf. Unmanned Sys. Tech.*, Kissimee, FL, 2006, pp. 109–114.

[15] D. Braganza, D. Dawson, I. Walker, and N. Nath, "A neural network controller for continuum robots," *IEEE Trans. Robot.*, vol. 23, no. 6, pp. 1270–1277, Dec. 2006.

[16] T. Mahl, A. Hildebrandt, and O. Sawodny, "A variable curvature continuum kinematics for kinematic control of the bionic handling assistant," *IEEE Transactions on Robotics*, vol. 30, no. 4, pp. 935–949, 2014.

[17] B. Jones and I. Walker, "Kinematics of multisection continuum robots," *IEEE Trans. Robot.*, vol. 22, no. 1, pp. 43–57, Feb. 2006.

[18] H. Mochiyama and H. Kobayashi, "The shape jacobian of a manipulator with hyper degrees of freedom," in *Proc. IEEE Int. Conf. Robot. Autom.*, Detroit, MI, 1999, pp. 2837–2842.

[19] I. Gravagne and I. D. Walker, "Manipulability, force, and compliance analysis for planar continuum manipulators," *IEEE Trans. Robots. Autom.*, vol. 18, no. 3, pp. 263–273, Jun. 2002.

[20] B. Jones and I. Walker, "A new approach to jacobian formulation for a class of multi-section continuum robots," in *Proc. IEEE Int. Conf. Robot. Autom.*, Barcelona, Spain, 2004, pp. 3279–3284.

[21] B. A. Jones, W. McMahan, and I. D. Walker, "Design and analysis of a novel pneumatic manipulator," in *Proc. IFAC Symposium on Mechatronic Systems*, Sydney, Australia, 2004, pp. 745–750.

[22] G. Chirikjian, "Hyper-redundant manipulator dynamics: A continuum approximation," *Adv. Robot.*, vol. 9, no. 3, pp. 217–243, Jun. 1995.

[23] G. Gallot, O. Ibrahimand, and W. Khalil, "Dynamic modeling and simulation of a 3-d eel-like robot," in *Proc. IEEE Int. Conf. Robot. Autom.*, Rome, Italy, 2007, pp. 1486–1491.

[24] R. Kang, A. Kazakidi, E. Guglielmino, D. Branson, D. Tsakiris, J. Ekaterinaris, and D. Caldwell, "Dynamic modeling of a hyper-redundant octopus-like manipulator for underwater applications," in *Proc. IEEE/RSJ Int. Conf. Intel. Robot. Syst.*, San Francisco, CA, 2011, pp. 4054–4059.

[25] A. Marchese, R. Tedrake, and D. Rus, "Dynamics and trajectory optimization for a soft spatial fluidic elastomer manipulator," in *Proc. IEEE Int. Conf. Robot. Autom.*, Seattle, WA, 2015, pp. 2528–2535.

[26] H. Mochiyama and T. Suzuki, "Kinematics and dynamics of a cable-like hyper-flexible manipulator," in *Proc. IEEE Int. Conf. Robot. Autom.*, Taipei, Taiwan, 2003, pp. 3672–3677.

[27] E. Tatlicioglu, I. Walker, and D. Dawson, "Dynamic modeling for planar extensible continuum robot manipulators," *Int. Jour. Robot. Autom.*, vol. 24, no. 4, pp. 1087–1099, Apr. 2009.

[28] S. M. H. Sadati, S. E. Naghibi, A. Shiva, I. D. Walker, K. Althoefer, and T. Nanayakkara, "Mechanics of continuum manipulators, a comparative study of five methods with experiments," in *Conf. Towards Autonomous Robotic Systems*, Y. Gao, S. Fallah, Y. Jin, and C. Lekakou, Eds. Guildford, UK: Springer, Cham, 2017, pp. 689–702.

[29] R. Goldman, A. Bajo, and N. Simaan, "Compliant motion control for multisegment continuum robots with actuation force sensing," *IEEE Trans. Rob.*, vol. 30, no. 4, pp. 890–902, Apr. 2014.

[30] A. Kapadia, K. Fry, and I. Walker, "Empirical investigation of closed-loop control of extensible continuum manipulators," in *Proc. IEEE Int. Conf. Intell. Robot. Sys.*, Chicago, IL, 2014, pp. 329–335.

[31] V. Falkenhahn, A. Hildebrandt, R. Neumann, and O. Sawodny, "Model-based feedforward position control of constant curvature continuum robots using feedback linearization," in *Proc. IEEE Int. Conf. Robot. Autom.*, Seattle, WA, 2015, pp. 762–767.

[32] S. Sadati, Y. Noh, S. Naghibi, and A. Althoefer, "Stiffness control of soft robotic manipulators for minimally invasive surgery (mis) using scale jamming," in *Int. Conf. Rob. and Autom.*, Amsterdam, The Netherlands, 2015, pp. 141–151.

[33] M. Yip and D. Camarillo, "Model-less feedback control of continuum manipulators in constrained environments," *IEEE Trans. Rob.*, vol. 30, no. 4, pp. 880–888, Apr. 2014.

[34] B. Conrad and M. Zinn, "Closed loop task space control of an interleaved continuum rigid manipulator," in *Proc. IEEE Int. Conf. Robot. Autom.*, Seattle, WA, 2015, pp. 1743–1750.

[35] S. M. H. Sadati, S. E. Naghibi, I. D. Walker, K. Althoefer, and T. Nanayakkara, "Control space reduction and real-time accurate modeling of continuum manipulators using ritz and rtiz-galerkin methods," *IEEE Robot. and Autom. Letters*, vol. 3, no. 1, pp. 328–335, Jan. 2018.

[36] M. Csencsits, B. Jones, and W. McMahan, "User interfaces for continuum robot arms," in *Proc. IEEE Int. Conf. Intell. Robot. Sys*, Edmonton, Canada, 2005, pp. 3011–3018.

[37] C. Frazelle, A. Kapadia, K. Fry, and I. Walker, "Teleoperation mappings from rigid link robots to their extensible continuum counterparts," in *Proc. IEEE Int. Conf. Robot. Autom.*, Stockholm, Sweden, 2016.

[38] A. Kapadia, I. Walker, and E. Tatlicioglu, "Teleoperation control of a redundant continuum manipulator using a non-redundant rigid-link master," in *Proc. IEEE Int. Conf. Intell. Robot. Sys.*, Algarve, Portugal, 2012, pp. 3105–3110.

[39] J. Hartranft, "Nonlinear model based control of robotic systems," Master's thesis, Clemson University, 2000.

[40] Y. Huang and T. Kuo, "Robust control for nonlinear time-varying systems with application to a robotic manipulator," *Int. J. of Sys. Sci.*, vol. 33, no. 10, pp. 831–837, 2002.

[41] A. Behal, W. Dixon, D. Dawson, and B. Xian, *Lyapunov-Based Control of Robotic Systems*. Boca Raton, FL, USA: CRC Press, 2009.

[42] A. Kapadia, I. Walker, D. Dawson, and E. Tatlicioglu, "A new approach to extensible continuum robot control using the sliding-mode," *Intl. J. Comp. Tech. and App.*, vol. 2, no. 4, pp. 293–300, 2011.

[43] C. Frazelle, A. Kapadia, and I. Walker, "Developing a kinematically similar master device for extensible continuum robot manipulators," in *Proc. of ASME IDETC on Mech. and Rob.*, Cleveland, OH, 2017.

[44] F. L. Lewis, D. M. Dawson, and C. T. Abdallah, *Robot Manipulator Control: Theory and Practice*. New York, NY: Marcel Dekker, 2004.

[45] MathWorks. (2016, April) Simulation and model based design. [Online]. Available: http://www.mathworks.com/products/simulink

[46] Quanser. (2015, September) Q8-usb data acquisition board. [Online]. Available: http://www.quanser.com/products/q8-usb